Brightness versus roughness: a multiscale approach

Maxence Bigerelle, Julie Marteau, C Paulin

Brightness versus roughness: a multiscale approach

M Bigerelle[1], **J Marteau**[1] **and C Paulin**[2]

[1] Laboratoire d'Automatique, de Mécanique et d'Informatique industrielles et Humaines (LAMIH), UMR-CNRS 8201, Université de Valenciennes et du Hainaut Cambrésis, Le Mont Houy, 59313—Valenciennes Cedex 9, France

[2] Industrial partner

E-mail: maxence.bigerelle@univ-valenciennes.fr

Keywords: roughness, multiscale, brightness

Abstract

A link between roughness and brightness is sought for brass specimens that were superfinished, sandblasted and brushed. Only the blasting conditions are varied in order to get different roughness and brightness. First, a relation between roughness and brightness is sought for specimens that were superfinished and sandblasted. The best relation is obtained using the mean height of the motifs, calculated using a low-pass filter and cut-off length equal to 30 μm, with a logarithmic–logarithmic model. Then, the same type of relation is determined after superfinishing sandblasting and brushing. The core material volume V_{mc}, computed using a high-pass filter with a cut-off length of 60 μm and a linear–logarithmic relationship, gives the best results. A relation between roughness and brightness that is common to both the pre-brushing state and post-brushing state is identified: the best roughness parameter is the arithmetic mean deviation S_a using a high-pass filter with a cut-off of 15 μm, with a logarithmic–logarithmic relationship. Finally, it is shown that the use of these filtering conditions enables us to verify the model of Beckmann and Spizzichino for the examined specimens. This scale corresponds to the end of the fractal regime and is close to the end of the signal correlation.

Nomenclature

A	Scattering zone area
B	Brightness
c	Normalized correlation length
h	Normalized root mean square surface height
I	Scattered intensity in the direction of the specular reflection
I_0	Intensity of the incident radiation
k	Constant
L_{ac}	Correlation length of the surface
l_x	Observation scale
l_y	Fixed range of the profile height
r_c	Curvature radius
R_t	Maximum range of amplitude of the profile
S_a	Arithmetic mean deviation
S_{bi}	Bearing index
S_{dc}	Material volume height difference
S_{dq}	Root mean square surface slope
S_{ds}	Density of summits
S_{fd}	Fractal dimension of the surface
S_{mr}	Material volume ratio
S_{pd}	Density of peaks
S_{pk}	Reduced peak height
S_{pq}	Root mean square slope of the plateau
S_q	Root Mean Square roughness
S_t	Total height of the surface
S_v	Maximum depth of the valley
S_{vk}	Reduced valley height
S_{5V}	Five-point peak height
V_m	Material volume
V_{mc}	Core material volume
V_v	Void volume
δ_x	Sampling interval
Δ_s	Fractal dimension
θ	Incident angle
λ	Wavelength

1. Introduction

Today, society places great value on product aspects as well as on body aesthetics. Materials contained in everyday products are thought to convey particular sensations and feelings to users [1, 2] and this can make taking on new products difficult (e.g. bioplastics acceptance [3]). Many studies are dedicated to aspect and gloss, which are particularly important for consumers. These studies cover areas such as paint and coatings [4–8], building stone tiles [9], cold-rolled steel strips [10], copper [11], aluminum [12, 13], automobile interior surfaces [14], dental materials [15], chocolate [16], paper [17], …

The link between roughness and brightness, or gloss, is particularly important as some studies showed, for example, that subjects' judgments of surface roughness was biased by illumination [18]. Indeed, frontal illumination makes surfaces appear smoother than glancing illumination angles. Other studies underlined the relationship between roughness and gloss [19, 20] or even developed optical inspection systems for quickly measuring surface roughness of thin films [21] and *vice versa* [22]. Most of the studies use roughness amplitude parameters such as the arithmetic mean value (R_a), or the root-mean square roughness (RMS or R_q) in order to find relationships between the surface topography and its reflectance characteristics, e.g. [23–28]. The latter are valued because they are easy to calculate and understand. However, these parameters may be limited and insufficient to describe the link between roughness and light reflection. Moreover, these parameters are often associated with a single cut-off filter, which may not correspond to the relevant scale of study. Järnström *et al* [29] argued that, while roughness is an intrinsic property of a surface, measured roughness is an extrinsic property as it is scale-dependent. Thus, they examined the effect of sampling interval, image size and filtering on the depiction of surface roughness. It enabled them to characterize roughness at different length scales and to identify the most relevant length scale for the correlation of R_q and gloss.

This paper aims to determine the most relevant roughness parameter and scale for the description of the brightness of brass components that were either superfinished and sandblasted (State 1) or superfinished, sandblasted and brushed (State 2). Finally, we search for the best roughness parameter and scale for the depiction of the link between roughness and brightness for both states.

2. Materials and methods

2.1. Specimens

The mechanical components are made of brass. Their final topography is the result of a combination of superfinishing, sandblasting and brushing. The choice of material and process was due to sensorial application.

In order to examine the effect of brushing, specimens that are superfinished and sandblasted are first examined. Then, the whole combination of processes (superfinishing + sandblasting + brushing) is analyzed.

For the specimens that were sandblasted, only the pressure and shot angle are varied. Duration and nozzle distance are constant. Ten configurations of processing parameters are studied using five pressure values and two values of angle. The processing parameters of superfinishing and brushing are the same for all the specimens.

2.2. Brightness measurements

Gloss is obtained by integrating the total amount of light reflected in the equal and opposite angle directions (called the specular direction) from a test area on a sample surface. Gloss of brass surface was measured using a small-area glossmeter (Novo-Curve, Rhopoint Instrumentation, East Sussex, United Kingdom) with a square measurement area of 2 mm × 2 mm and 60° geometry. Gloss measurements are hereafter expressed in gloss units (GU). The reproducibility is equal to 0.5 GU and the repeatability is equal to 0.2 GU for values of gloss below 200 GU. Ten measurements were made on each specimen.

2.3. Roughness measurements

The specimen topography was measured using an optical profiler (WYKO NT9300, VEECO, United States) with a x100 objective. The surface area is equal to 127 μm × 92 μm. The configuration gave a lateral resolution equal to 0.22 μm and a vertical accuracy of about 1 nm.

2.4. Multiscale decomposition of roughness

Surface topography is analyzed using a multiscale analysis. Fifty roughness parameters were assessed using twenty-one cut-off lengths and three types of Robust Gaussian filters [30]: a high-pass, a low-pass and a band-pass filter.

The roughness parameters are:

(i) Amplitude parameters [31]: the arithmetic mean deviation S_a, the root-mean-square deviation S_q, the total height of the surface S_t, the maximum depth of valleys S_v, …

(ii) Hybrid parameters [31]: the density of summits S_{ds}, the fractal dimension of the surface S_{fd}, the root-mean-square slope of the surface S_{dq}, …

(iii) Area and volume parameters [32]: the material volume ratio S_{mr}, the material volume height difference S_{dc}, Material volume V_m, void volume V_v, …

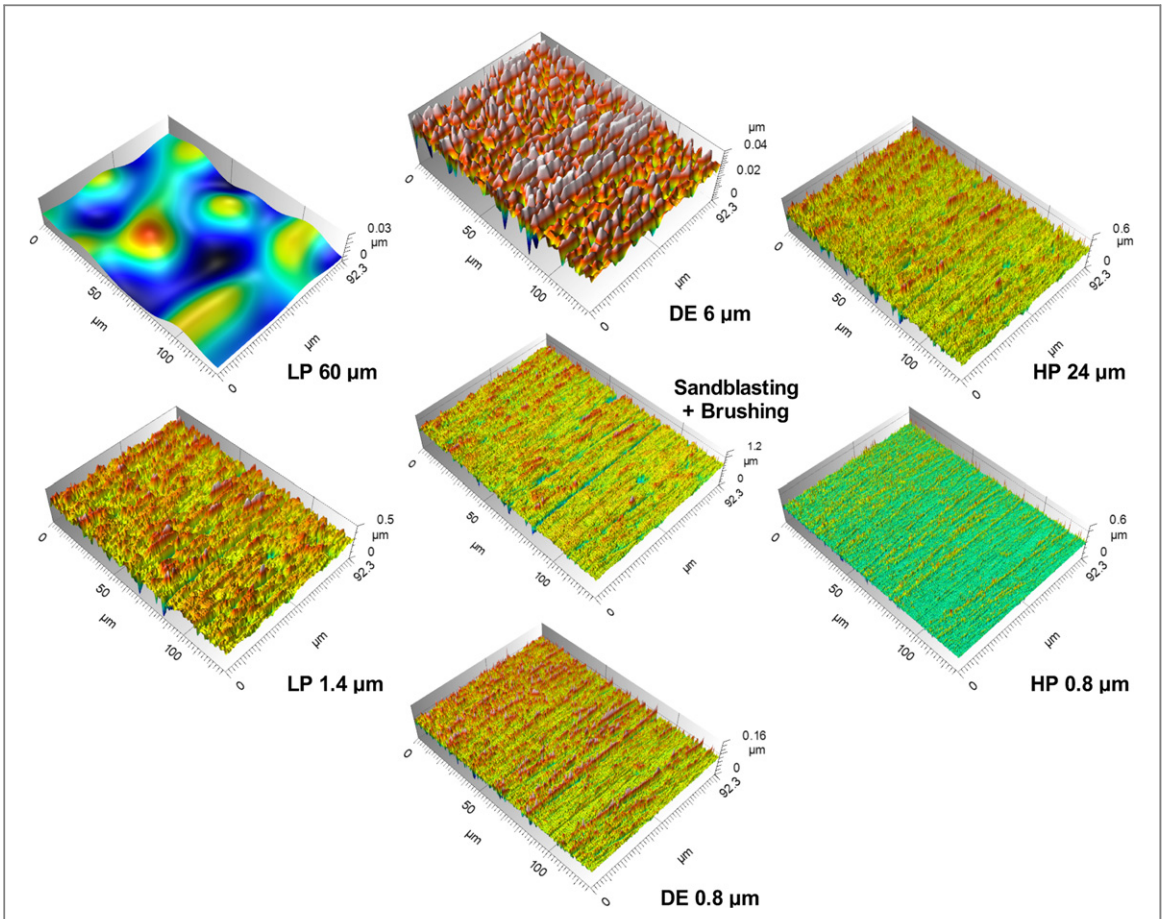

Figure 1. Multiscale decomposition of a surface that was superfinished, sandblasted and brushed, using a low-pass filter (LP) with cut-off lengths equal to 60 μm and 1.4 μm, a band-pass filter (DE) with cut-off lengths equal to 6 and 0.8 μm and a high-pass filter (HP) with cut-off lengths equal to 24 and 0.8 μm.

(iv) Feature parameters [32]: Density of peaks S_{pd}, Five-point pit height S_{5V}, … All these parameters are determined using segmentation (watershed algorithm). The latter enables us to identify the main motifs (significant peaks and holes) of a surface.

(v) Functional parameters [33]: Reduced peak height S_{pk}, Reduced valley depth S_{vk}, Plateau root-mean-square roughness S_{pq}, bearing index S_{bi}, …

It is worth noting that many of these parameters are dimensionally dependent and that some are more robust than others. During the analysis, dimensionless ratios of these roughness parameters were also tested. However, the results are hereafter focused on the results of the roughness parameters of standards and the results of these dimensionless ratios are not shown for the sake of brevity.

These parameters were computed using three types of robust Gaussian filters [30]: a low-pass filter, a high-pass filter and a band-pass filter. The following twenty-one cut-off lengths were used: 0.8, 1, 1.2, 1.4, 1.7, 2, 2.6, 3.1, 3.9, 4.8, 6, 7.5, 10, 13, 17, 24, 40, 60 and 120 μm. The choice of cut-off values is based on a geometric progression. Figure 1 illustrates the use of a high-pass filter, a low-pass filter and a band-pass filter on the surface of a specimen that was superfinished, sandblasted and brushed. For the band-pass filter, the indicated cut-off length corresponds to the first cut-off of the filter and the bandwidth is equal to the subtraction of this value from the next larger cut-off length. As an example, the label 'DE 6 μm' means that the first cut-off of the used band-pass filter is equal to 6 μm and the bandwidth is equal to (7.5–6) = 1.5 μm. Low-pass filters enable us to study waviness while the high-pass filters are used to analyze surface microroughness. Band-pass filters are useful to study a range of frequencies. It will help us to determine of the best scale for the calculation of the roughness parameters.

2.5. Method for the determination of the best relation between roughness and brightness

Simulated bootstrap values were used in order to determine a relation between brightness and roughness. The term 'bootstrap' refers to the statistical technique that consists in generating a large number of simulated samples by randomly sampling with a replacement set of experimental values [10]. For the roughness values, the following steps were used:

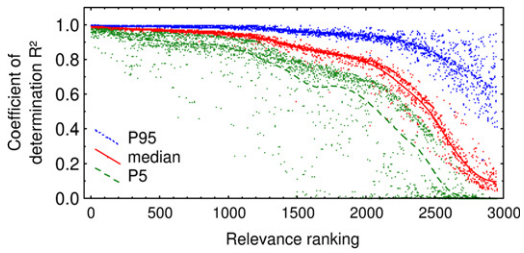

Figure 2. Coefficient of determination R^2 as a function of the relevance ranking, for the specimens that were superfinished and sandblasted.

(i) R surface measurements are randomly sampled with replacement,

(ii) All the roughness parameters are calculated for the R surfaces, using twenty-one cut-off lengths and three types of filters. The total number of roughness parameters (assessed using twenty-one cut-off lengths with three types of filters) is hereafter called Q.

(iii) The mean of each roughness parameter (associated with a cut-off length and a type of filter) is calculated.

These three steps are repeated until the number of required bootstraps is reached. Then, these bootstrapped values are used in order to determine an empirical probability density function. The same approach is applied to brightness measurements. A relation is then sought using the bootstrapped values of brightness and roughness. Four types of models are tested. They combine linear and logarithmic parts, thus giving linear–linear models, logarithmic–linear models, linear–logarithmic models and logarithmic–logarithmic models. The testing of four models using forty-nine roughness parameters calculated over twenty-one cut-off lengths using three types of filters implies that more than 10 000 combinations were assessed. The models were ranked according to the value of the coefficient of determination. The best model is the one showing the largest coefficient of determination.

3. Results

3.1. Superfinished and sandblasted specimens

First, the best relation between brightness and roughness was determined for the intermediate treatment (State 1) *i.e.* for the specimens that were only superfinished and sandblasted. Figure 2 shows the median, the 5th percentile and the 95th percentile of the coefficient of determination R^2 as a function of the relevance ranking. The relevance ranking enables us to present the results from the highest median value to the lowest median value.

According to this ranking, the best model ($R^2 = 0.996$) was found when using a logarithmic–logarithmic model with the mean height of the motifs, calculated using a cut-off length of 30 μm and a low-pass filter. Motifs are topographic features determined using the watershed algorithm with a pruning criterion. Motifs are either hills (or dales) surrounded by course lines determined by the segmentation algorithm and having one extreme point: one peak (or pit). Figure 3 depicts the mean height of the motifs computed with a low-pass filter and a cut-off length of 30 μm as a function of brightness.

For high frequencies, the best parameter is the maximum depth of furrows calculated using a cut-off length equal to 30 μm with a high pass filter and a logarithmic–logarithmic model. The furrows are also determined using the watershed algorithm. Figure 4 shows the maximum depth of furrows computed with a high-pass filter and a cut-off of 30 μm as a function of brightness.

3.2. Superfinished, sandblasted and brushed specimens

The same methodology was applied to the measurements made on the specimens that were superfinished, sandblasted and brushed. Figure 5 shows the median, the 5th percentile and the 95th percentile of the coefficient of determination R^2 as a function of the relevance ranking. The largest coefficient of determination is equal to 0.987. The latter corresponds to the use of a linear–logarithmic relation with the core material volume V_{mc} computed using a high-pass filter and a cut-off length equal to 60 μm. This roughness parameter quantifies the volume of material comprising between heights located at material ratio values equal to $p = 10\%$ and $q = 80\%$.

Figure 6 depicts the core material volume V_{mc} computed using a high-pass filter with a cut-off length equal to 60 μm as a function of brightness. This roughness parameter is useful to understand how much material is available for load bearing after the removing of the top levels of the surface. The gradient images show that it is difficult to find the sandblasted characteristics on the specimens having brighter surfaces: polishing features are predominant.

For low frequencies, the most relevant roughness parameter is the root-mean-square surface slope S_{dq}, computed using a cut-off length approximately equal to 8 μm with a low-pass filter. Figure 7 shows this parameter as a function of brightness with a linear–logarithmic model. The S_{dq} parameter is a general measurement of the slopes which comprise the surface. Surfaces having the same similar average roughness can contain different slopes. The S_{dq} parameter can be used to differentiate them. The relevance of this parameter can be explained by its direct link with the polishing angle of attack.

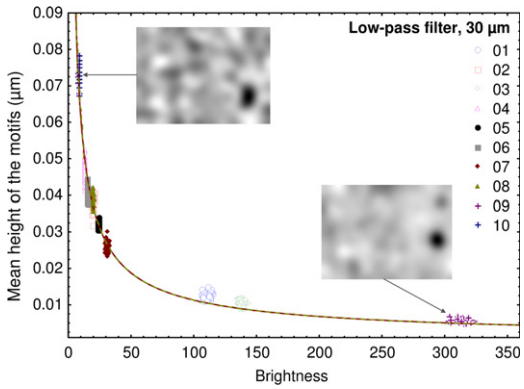

Figure 3. Mean height of the motifs as a function of brightness for the specimens that were superfinished and sandblasted. The mean height of the motifs was calculated using a low-pass filter with a cut-off length of 30 μm.

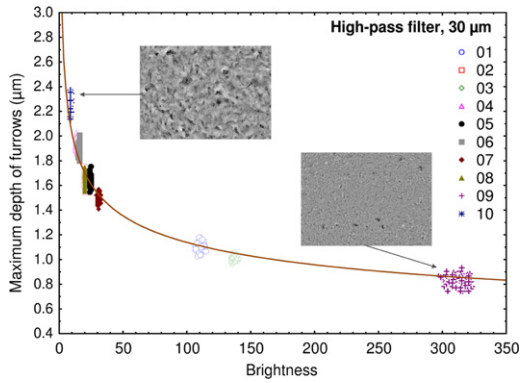

Figure 4. Maximum depth of the furrows as a function of brightness for the specimens that were superfinished and sandblasted. The maximum depth of the furrows was calculated using a high-pass filter with a cut-off length of 30 μm.

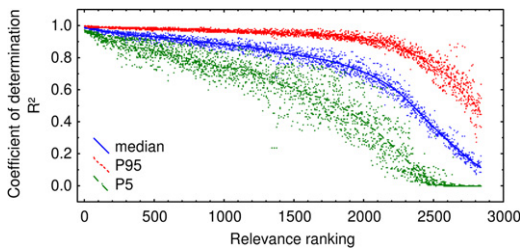

Figure 5. Coefficient of determination R^2 as a function of the relevance ranking for the specimens that were superfinished, sandblasted and brushed.

3.3. Determination of the best relation between roughness and brightness for both states

The previous computations enabled us to identify the best scale and roughness parameter for the description of the link between topography and brightness for each studied state i.e. for specimens that were superfinished and sandblasted (State 1) and for specimens that were superfinished, sandblasted and brushed (State 2). In order to examine the change of brightness due to brushing, one may need to use the same roughness parameter and scale for both states. Thus, a compromise is needed. Using the same methodology, the most relevant roughness parameter and scale for the description of the link between brightness and topography for both states was determined. The best roughness parameter is found by summing both F values i.e. the one found for the specimens that were superfinished and blasted and the one computed for the specimens that were superfinished, blasted and brushed. This new F-value is used to find the new ranking of the specimens. The best roughness parameter is the arithmetic mean deviation S_a, using a high-pass filter with a cut-off length equal to 15 μm and a logarithmic–logarithmic relation. Figures 8 and 9 show the arithmetic mean deviation S_a computed using a high-pass filter with a cut-off length of 15 μm as a function of brightness for State 1 and State 2, respectively. Figures 8 and 9 show that this parameter enables us to describe the brightness value reversal. Indeed, the brightness value of Specimen 9 is higher than that of Specimen 10 when they are only superfinished and sandblasted. Once these specimens are brushed, Specimen 9 becomes less bright than Specimen 10.

4. Discussion

The previous section showed that the best relation between roughness and brightness can be given by different roughness parameters (associated with certain filtering conditions), depending on the examined states (superfinished + sandblasted or superfinished + sandblasted + brushed). However, when searching for a roughness parameter that is common to both states, it was shown that the arithmetic mean deviation S_a calculated at a certain scale is the best roughness parameter for the description of the relation between morphology and brightness. It is worth noting that one of the most used models for the description of the relation between surface morphology and brightness, or reflectance, is the one of Beckmann and Spizzichino [34], which uses the root-mean-square roughness (S_q) for the description of the examined morphology. The root-mean-square roughness S_q is an amplitude parameter that is equal to the arithmetic mean deviation S_a under Gaussian assumptions of height amplitude, ignoring a multiplication factor.

The model of Beckmann and Spizzichino is a physical model based on electromagnetic wave theory, which was built in order to predict the reflectance of surfaces having different roughness values. If this model can be used for the examined surfaces, then the brightness values would gain a physical meaning.

The model of Beckmann and Spizzichino is based on an evaluation of the Helmholtz integral and thus requires Kirchoff's approximation. A detailed

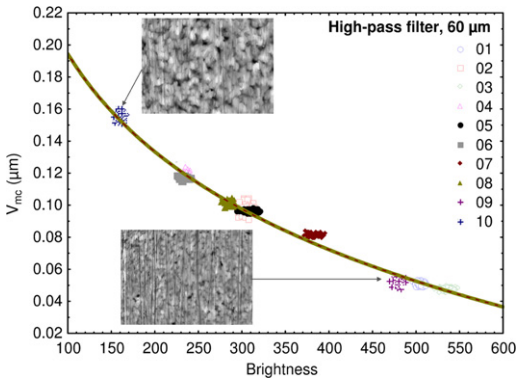

Figure 6. The core material volume V_{mc} as a function of brightness, for the specimens that were superfinished, sandblasted and brushed. The core material volume was calculated using a high-pass filter and a cut-off length equal to 60 μm.

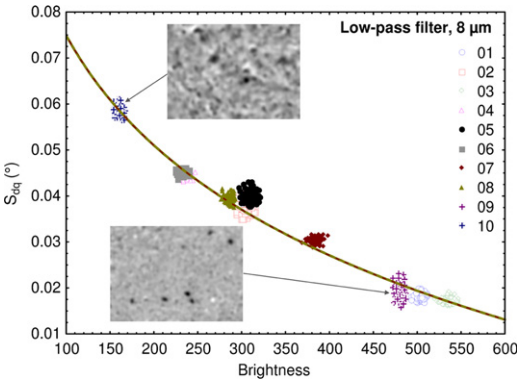

Figure 7. Root-mean-square surface slope S_{dq} as a function of brightness, for the specimens that were superfinished, sandblasted and brushed. The root-mean-square surface slope S_{dq} was calculated using a cut-off length of 8 μm with a low-pass filter.

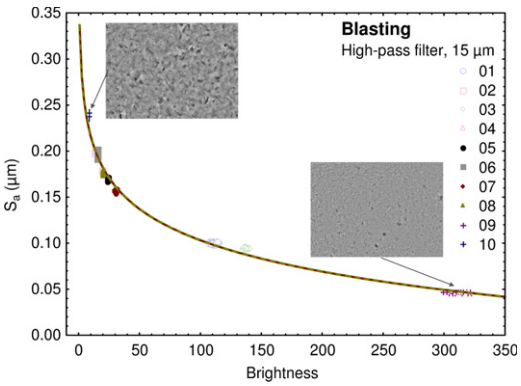

Figure 8. The arithmetic mean deviation S_a as a function of brightness, for the specimens that were superfinished and sandblasted. The arithmetic mean deviation was calculated using a high-pass filter and a cut-off length equal to 15 μm.

derivation of this model can be found in [34]. Only the main principles and assumptions are highlighted hereafter. During the derivation of this model, the following assumptions are made:

- Assumption A: the radius of curvature of surface irregularities is large compared to the wavelength of incident light (Kirchoff's assumption). It means that the surface does not have any sharp edges or points (compared to the wavelength of incident light). This assumption is necessary to approximate the electromagnetic field: the field at a point on the surface can be approximated by the field that would be present on a tangent plane at that point.

- Assumption B: mutual interaction of surface irregularities may be neglected (masking and shadowing of surface points by adjacent surface points is ignored),

- Assumption C: there are no multiple scatterings: the incident wave is reflected only once. It does not bounce between surface points before scattering.

- Assumption D: only the far field is calculated. The incident wave is assumed to be a plane wave,

- Assumption E: the height amplitude of roughness (surface height) follows a Gaussian density,

- Assumption F: roughness amplitude correlation follows a given analytical formula (exponential, Gaussian…).

Considering these assumptions for perfectly conducting rough surfaces generated by random processes (such surfaces can be described using their Gaussian statistical distributions and correlation function), Beckmann [34] found the following formula from a calculation of the Helmholtz integral:

$$\frac{I}{I_0} = \exp\left(-\left(\frac{4\pi S_q \cos\theta}{\lambda}\right)^2\right) + \frac{\lambda^2 {L_{ac}}^2}{16\pi A {R_q}^2 \cos\theta} \quad (1)$$

where I/I_0 represents the ratio of the scattered intensity in the direction of the specular reflection I to the intensity of the incident radiation I_0, λ is the wavelength, θ is the incident angle, A the scattering zone area, S_q is the Root Mean Square roughness and L_{ac} is the correlation length of the surface. In the previous equation, the ratio I/I_0 increases when S_q decreases or when L_{ac} increases. It means that the ratio I/I_0 increases when the surface is smoother.

Several models are based on the pioneering works of Beckmann and Spizzichino. Most of these models express the scattered intensity of an optical wave as a function of the scattering angle, the electromagnetic properties of the studied material, the wavelength and commonly used surface parameters such as S_q and L_{ac}.

It must be pointed out that these models were developed for periodical (sinusoidal or saw-tooth profiles) and random surface roughness. Nevertheless, more recently, wave interactions with fractally rough surfaces have been also studied [35–41].

Several authors also used Kirchhoff's assumption in their work in order to describe the optical properties

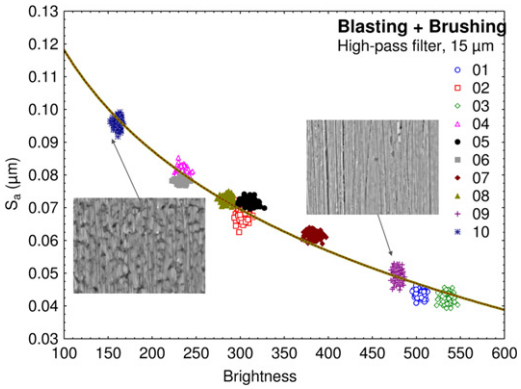

Figure 9. The arithmetic mean deviation S_a as a function of brightness, for the specimens that were superfinished, sand-blasted and brushed. The arithmetic mean deviation was calculated using a high-pass filter and a cut-off length equal to 15 μm.

of fractal structures. For example, Jaggard [35] developed a method for remotely characterizing the fractal dimension of a surface using the Kirchhoff method for the calculation of the distribution of the scattered energy as a function of the scattering angle, for different types of surface roughness. He showed that, as the fractal dimension of the surface increases, surface roughness increases and more scattered energy spreads away from the specular direction. Similarly, Sheppard [36] predicted that, for a rough two-dimensional surface having stationary statistics and normal distribution of the heights, the scattering varies with $c/h^{2/(3-\Delta s)}$, where c and h can be seen as the normalized correlation length and the normalized Root Mean Square surface height respectively and Δ_s is the fractal dimension of the surface. The latter can vary between 2 and 3. A fractal dimension Δ_s equal to 2 corresponds to an ideally smooth surface while a fractal dimension equal to 3 corresponds to a rough surface. However, Sheppard's theoretical work was not confirmed by experimental works.

Moreover, as outlined by Jakeman [37], a Gaussian random fractal surface, though continuous, is not differentiable. Thus, the notion of a tangent plane required to estimate the Hemholtz integral (the scattered intensity) within Kirchhoff approximations doesn't exist anymore for a fractal representation of surface roughness. This conclusion is in agreement with Botet *et al* [39] who claimed that neither Rayleigh's perturbation approximation nor Kirchhoff's approach can be applied to describe optical properties of a fractal self-affine structure.

In their work, Botet *et al* [39] adopted the microscopic 'discrete–dipole approximation' (DDA) initially suggested by Purcell and Pennypacker [40] and lately developed by Draine [41] in order to calculate the optical response from an object of an arbitrary shape. They numerically generated a surface with a self-affine fractal structure similar to the one of a cold deposited metal one, treating it as a collection of N linear polarizable particles with a linear size assumed to be much smaller than the wavelength. They showed that for a self-affine fractal surface, the spatial distribution of the local field (or the scattered intensity) is extremely inhomogeneous and that the non-linear optical responses are dramatically enhanced compared to those of smooth interfaces.

These results show that the length of the considered asperities compared to the wavelength should be carefully considered before using electromagnetic wave theory. Yet, the characterization of the geometry of the asperities remains an important issue. A large number of authors suggest applying Kirchhoff hypothesis in order to determine the curvature radius. They also postulate that the curvature radius r_c must be larger than the wavelength λ. As an example, Brekhovskikh [42] suggested that $4\pi r_c \cos\theta \gg \lambda$. Nowicki [43] proposed a method for directly determining the asperity radius r_c from the surface. His method is based on the description of a peak, as shown in figure 10. The curvature radius r_c is equal to:

$$r_c = \frac{l_x^2}{8l_y}, \tag{2}$$

with $l_y = 0.1R_t$ or $l_y = 0.05R_t$, where R_t is the maximum range of amplitude of the profile. This method consists in finding the radius of a circle passing through three points x_l, x_r and x_m, assuming that $l_y \ll l_x$.

The following should be considered:

(i) The technique used for the detection of peaks is not well defined. Nowicki determined all the local peaks for a fixed l_y value (in a discretized case, if $z_{i-1} < z_i$ and $z_i > z_{i+1}$ then z_i is a peak. As l_y is fixed, a unique value of l_x is found for each peak, thus giving a discretized set of points $\{z_{i-q}, \ldots, z_{i-1}, z_i, z_{i+1}, z_{i+2}, \ldots, z_{i+p}\}$. The peak is retained if $z_{i-q} < \ldots < z_{i-2} < z_{i-1} < z_i$ and $z_i > z_{i+1} > z_{i+2} > \ldots > z_{i+p}$. The analytical method assumes that z_i is the maximum peak of the non-discretized surface and implies that the peak has a perfect circular shape if $p = q$. Thus, if $p \neq q$ then the peaks do not have a perfect circular shape.

(ii) The choice of the threshold used to estimate $l_y = \alpha R_t$ has no theoretical justifications. As the radius of the asperity is the sought parameter, one must have $l_y = \lim_{\alpha \to 0} \alpha R_t$. However, with the use of discretized curves, this will lead to the indeterminacy of the l_x values for small l_y, as $l_x = k\delta_x$ where δ_x is the sampling interval. Furthermore, due to the stochastic aspect of the profile, as the value of l_y decreases, the three points x_l, x_r and x_m tend to become collinear and thus it dramatically

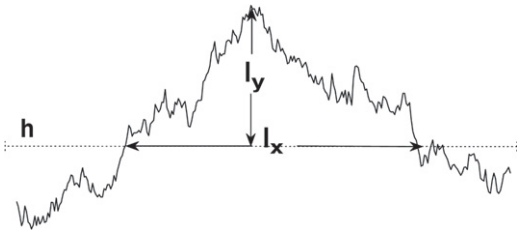

Figure 10. Description of a peak on a stochastic profile measured at the intercept at level h where l_x and l_y are evaluated.

increases the variance estimator of the curvature radius.

(iii) A large number of physical surfaces are fractal [44–50]. However, the calculation of the curvature radius on fractal surfaces has no physical meaning. Applying Nowicki's method will lead to different values of r_c as it depends on the sampling rate. Indeed, decreasing the sampling rate will decrease the curvature radius r_c. It means that calculating r_c using Nowicki's method will have no meaning if it is postulated that $z_{i-q} < \cdots < z_{i-2} < z_{i-1} < z_i$ and $z_i > z_{i+1} > z_{i+2} > \cdots > z_{i+p}$. Thus, the concept of curvature radius r_c must be redefined.

The curvature radius r_c of fractal curves has a physical meaning when scales are used. Thus, the curvature radius could be defined for a given scale. Nowicki's method needs to be corrected. In this new definition, the concept of l_x values will be kept but no points of the profile belonging to l_x intervals will have to meet any criteria. As previously explained, the values of α cannot be fixed without introducing artefacts. For this reason, the value of r_c is calculated using the following method:

(1) A horizontal line, crossing the profile at a given height h, is chosen. Then, a set of l_x values, crossing this horizontal line, is calculated.

(2) For each l_x value, the local maximum peaks are computed thus giving l_y values.

(3) The curvature radius r_c is then computed using equation (2) for each element.

(4) Another horizontal line, crossing the profile at a given height h, is chosen and steps 1 to 3 are repeated.

It was proved [51] that, for all the non-constant continuous functions uniformly Hölderian and anti-Hölderian f, defined on $[a,b]$, if l_x exists then:

$$\Delta(f, a, b) = \lim_{l_x \to 0} \sup\left(\log r_c\left(l_x\right)/\log l_x\right). \quad (3)$$

Polishing profiles have been shown to have these properties [52]. For all the profiles, $\log r_c\left(l_x\right)$ was plotted as a function of $\log l_x$. That represents more than 3 000 000 values of $\log r_c\left(l_x\right)$. In order to visualize these curves, the mean of $\log r_c\left(l_x\right)$ is computed for intervals of l_x equal to 1 μm, as shown in figure 11. It is worth noting that some of the well-known parameters, such as the slope and curvature, cannot be defined for fractal surfaces. However, a close approximation is often acceptable for numerical purposes. According to equation (2), the experimental data can be fitted using the following relationship:

$$\log r_c\left(l_x\right) = \log r_{c0} + \Delta \log l_x \quad (4)$$

As shown in figure 12, equation (4) can be used for fitting the experimental data. The previously defined mathematical assumptions are satisfied for all the samples. Thus, the curvature radius has indeed a meaning at the scale at which it is observed. The curvature radius increases as the observation scale l_x increases.

In order to verify Assumption A, the probability density functions of the radii of curvature r_c of all the specimens that were superfinished, sandblasted and brushed are plotted. It can be seen in figure 13 that the radii of curvature are larger than the bandwidth of the studied wavelight.

The Gaussian probability density functions of the curvature radius and the amplitude should be analyzed in order to verify the initial assumptions. Figure 14 shows the mean probability density function of the amplitude of the surface roughness, for the specimens that were superfinished, sandblasted and brushed. All the mean probability functions have a Gaussian distribution with a mean equal to zero. As a consequence, only the standard deviation of the roughness amplitude (i.e. the Root Mean Square roughness parameter S_q) describes the roughness amplitude and a Gaussian model can be applied in Beckmann's model. As for the autocorrelation function, it is better described using an exponential model than a Gaussian function, as shown in figure 15. However, the fitting error for the Gaussian model remains acceptable. In order to compare the results to the one given by Beckmann's model, the autocorrelation function will be considered Gaussian.

Therefore, both assumptions D and F are satisfied for rough surfaces: Beckmann's model can be applied.

Now, let's find out if Beckmann's model can be validated using the experimental data of superfinished, sandblasted and brushed surfaces. First, it is assumed that roughness can be described by specular lobes. Thus, equation (1) can be written as follows:

$$\frac{I}{I_0} = \exp\left(-\left(\frac{4\pi S_q \cos\theta}{\lambda}\right)^2\right). \quad (5)$$

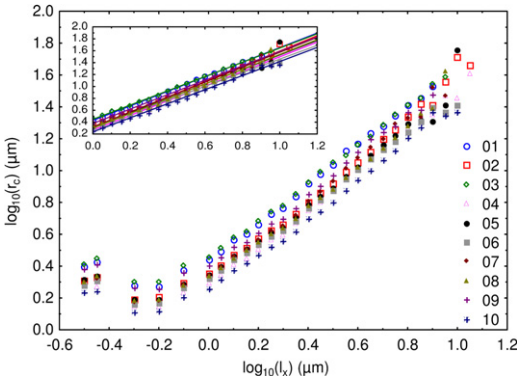

Figure 11. Influence of the polishing method on the evolution of $\log r_c\left(l_x\right)$ versus $\log\left(l_x\right)$, for all the specimens that were superfinished, sandblasted and brushed. The linear regression lines give the fractal dimension.

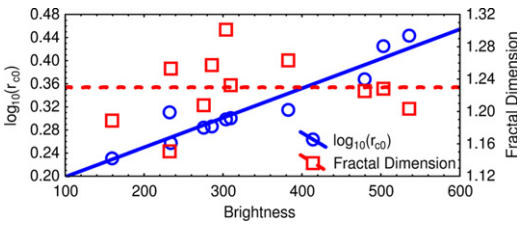

Figure 12. Mean of the curvature radius r_{c0} and fractal dimension as a function of brightness.

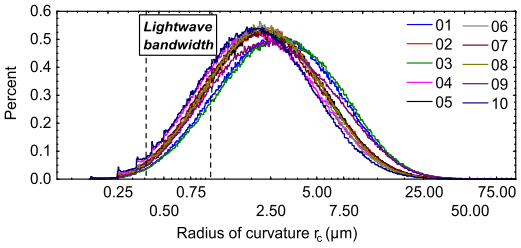

Figure 13. Probability density functions of the radii of curvature of the specimens that were superfinished, sandblasted and brushed.

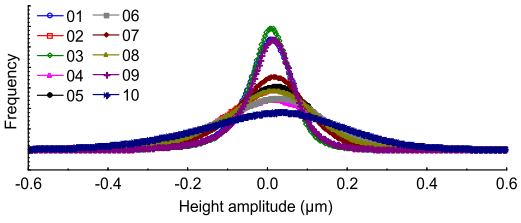

Figure 14. Probability density functions of the roughness amplitude of the specimens that were superfinished, sandblasted and brushed.

For a log–log plot, the previous equation becomes:

$$\log_{10}\frac{I}{I_0} = \frac{1}{2.3}\left(-\left(\frac{4\pi S_q\cos\theta}{\lambda}\right)^2\right) \cong -\frac{17}{\lambda^2}{S_q}^2. \quad (6)$$

It should be pointed out that the gloss meter measures brightness using the reflection of an internal mirror. This mirror is not perfect. This is highlighted by the experimental data values: all the brightness values are larger than 100%. The brightness B determined by the glossmeter is lower than the ideal reflection by a factor k ($k > 1$) given by I/I_0 *i.e.* $kI/I_0 = B$. For a perfectly reflected light ($S_q = 0$), the constant k is equal to B.

Using the mean lightwave of the light source (equal to 0.56 μm), equation (6) becomes:

$$\log_{10} B \cong -50{S_q}^2 + \log_{10} k. \quad (7)$$

Figure 16 depicts the coefficient of determination R^2 as a function of the scale i.e. the cut-off length. The best relationship is found using a high-pass filter with a cut-off length of 15 μm. This relationship is well-defined for high frequencies and when omitting the low frequencies of the surface. This means that specular reflection occurs at high frequency: as the values in this functional application are small, surface waviness does not influence gloss.

Another important and original result is obtained: it can be observed that the S_q values must be computed at a scale corresponding to a non-fractal regime. Indeed, the cut-off length represents the length from which the surface is statistically ergodic. This trend can be clearly seen in the first graphs of this article. Once this threshold is exceeded, the S_q values do not follow the classical fractal relation anymore. This threshold also corresponds to the end of the fractal regime of the curvature radius: it can be seen in figure 11 that the curvature radius becomes constant ($10^{1.2} = 15\,\mu$m). Finally, this threshold is also close to the end of the correlation of the signal (figure 15). This clearly means that the roughness parameter used to assess the specular component of the scattering must be computed with a filter that includes all the high frequencies of the topography, until the signal becomes ergodic and gives the threshold of the filter. The cut-off can be determined using the log-log plot of the considered roughness parameters including the fractal aspect of the surface morphology.

The equations of regression obtained at this maximum value of relevance are now analyzed. The following equation is obtained:

$$\log_{10} B \cong -44{S_q}^2 + 2.91. \quad (8)$$

The slope of the previous equation (equal to −44) is close to the theoretical value given by Beckmann's theory (equal to −50). In order to validate the previous approach, this slope is computed for different cut-off values using a low-pass and a high-pass filter. Figure 17

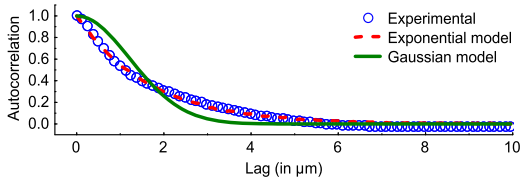

Figure 15. Mean autocorrelation function for Specimen 8, fitted using an exponential model and a Gaussian model.

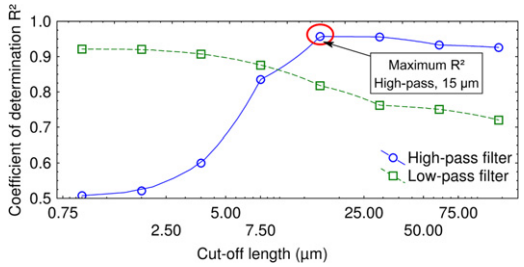

Figure 16. Coefficient of determination R^2 obtained by the least square method for the computation of equation (7) as a function of the cut-off lengths, using a high-pass and a low-pass filter.

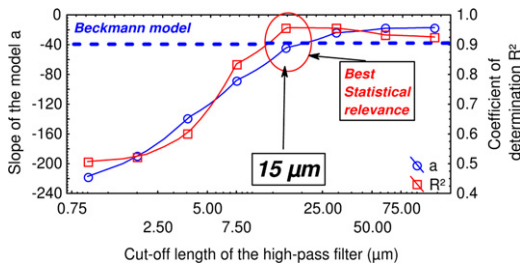

Figure 17. Analysis of the coefficient of determination and slope of the model $\log_{10} B \cong -aS_q{}^2 + \beta$ obtained by fitting equation (1) using the least square method, as a function of the high-pass filter cut-off length.

depicts the value of this slope and the value of the coefficient of determination as a function of the cut-off length for a high-pass filter. The best relevance is found for a slope value equal to the value computed using Beckmann's model. Any other cut-off length will lead to a value that does not match Beckmann's model. Therefore, all the previous remarks are validated. The identified cut-off value was found when searching for a relation between the measured topography and brightness, without including the process parameters into the analysis. The modeling of blasting and brushing in order to link the topography with the process parameters will be the subject of a future paper.

Using the results of this section, the brightness of the specimens that were superfinished, sandblasted and brushed is plotted as a function of the Root Mean Square roughness S_q, as depicted in figure 18.

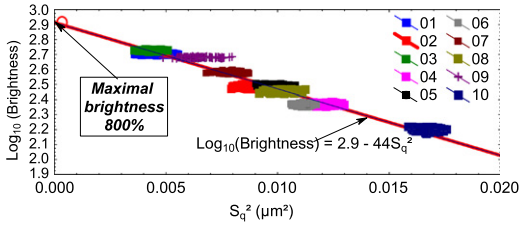

Figure 18. Brightness as a function of the mean square roughness parameter S_q, at the most relevant scale (high-pass filter, 15 μm).

5. Conclusion

This study aimed to determine the most relevant roughness parameter and scale for the depiction of the relationship between brightness and topography for specimens that were either superfinished and sandblasted (State 1), or superfinished, sandblasted and brushed (State 2).

For State 1, the most relevant parameter and scale was found to be the mean height of the motifs calculated using a low-pass filter with a cut-off length of 30 μm. For the high frequencies, the maximum depth of the furrows calculated using a high-pass filter with a cut-off length of 30 μm was identified as the best parameter.

For State 2, the most relevant parameter for the description of the link between topography and brightness was found to be the core material volume V_{mc} computed using a high-pass filter with a cut-off length equal to 60 μm. For the low frequencies, the best parameter was the root-mean-square surface slope S_{dq} calculated using a low-pass filter with a cut-off length of 8 μm.

The most relevant parameter for the description of the relationship between roughness and brightness using the same scale and parameter for State 1 and 2 was found to be the arithmetic mean deviation S_a computed using a high-pass filter with a cut-off length equal to 15 μm. This amplitude parameter is equal to another roughness parameter ignoring a multiplication factor (0.8): the root-mean-square roughness S_q. The latter is used in one of the most used physical model for the description of the link between morphology and brightness: the model of Beckmann and Spizzichino, based on the electromagnetic wave theory. This model was verified for the examined specimens and it was shown that the root-mean-square roughness S_q should be calculated using a high-pass filter with a cut-off length equal to 15 μm, which is the same relevant scale found when searching for a common parameter to both states. This scale corresponds to the end of the fractal regime of the curvature regime and is close to the end of the signal correlation.

References

[1] Karana E, Hekkert P and Kandachar P 2009 Meanings of materials through sensorial properties and manufacturing processes *Mater. Des.* **30** 2778–84

[2] Fleming R W 2014 Visual perception of materials and their properties *Vision Res.* **94** 62–75

[3] Karana E and Fiberness N N 2014 Reflectiveness and roughness in the characterization of natural and high quality materials *J. Cleaner Prod.* **68** 252–60

[4] Hennebelle F, Najjar D, Bigerelle M and Iost A 2006 Influence of the morphological texture on the low wear damage of paint coated sheets *Prog. Org. Coat.* **56** 81–9

[5] Najjar D, Bigerelle M, Hennebelle F and Iost A 2006 Contribution of statistical methods to the study of worn paint coatings surface topography *Surf. Coat. Technol.* **200** 6088–100

[6] Mezghani S, Zahouani H and Piezanowski J J 2011 Multiscale characterizations of painted surface appearance by continuous wavelet transform *J. Mater. Process. Technol.* **211** 205–11

[7] Savall C, Rebere C, Sylla D, Gadouleau M, Refait P and Creus J 2006 Morphological and structural characterisation of electrodeposited Zn—Mn alloys from acidic chloride bath *Mater. Sci. Eng.*, A **430** 165–71

[8] Scheers J, Vermeulen M, De Maré C and Meseure K 1998 Assessment of steel surface roughness and waviness in relation with paint appearance *Int. J Mach. Tools Manuf.* **38** 647–56

[9] Yavuz H, Ozkahraman T and Demirdag S 2011 Polishing experiments on surface quality of building stone tiles *Construct. Build. Mater.* **25** 1707–11

[10] Najjar D, Bigerelle M and Iost A 2003 The computer-based bootstrap method as a tool to select a relevant surface roughness parameter *Wear* **254** 450–60

[11] Awad A M, Ghany N A A and Dahy T M 2010 Removal of tarnishing and roughness of copper surface by electropolishing treatment *Appl. Surf. Sci.* **256** 4370–5

[12] Beck G and Funk S 2012 Correlation between optical appearance and orientation of aluminium *Surf. Coat. Technol.* **206** 2371–9

[13] Fairlie M and Timsit R S 1986 Light scattering from medium-gloss aluminium surfaces *Wear* **109** 29–42

[14] Maeda M, Kachi T, Ito H and Matsuda M 1997 Measurement of gloss for wrinkly textures of an automobile interior *Opt. Laser Technol.* **29**

[15] Alandia-Roman C C, Cruvinel D, Sousa A B S, Pires-de-Souza F C P and Panzeri H 2013 Effect of cigarette smoke on color stability and surface roughness of dental composites *J. Dentistry* **41** 73–9 (Suppl. 3)

[16] Briones V, Aguilera J M and Brown C 2006 Effect of surface topography on color and gloss of chocolate samples *J. Food Eng.* **77** 776–83

[17] Vernhes P, Bloch J-F, Mercier C, Blayo A and Pineaux B 2008 Statistical analysis of paper surface microstructure: a multiscale approach *Appl. Surf. Sci.* **254** 7431–7

[18] Ho Y X, Landy M S and Maloney L T 2006 How direction of illumination affects visually perceived surface roughness *J Vis.* **6** 634–48

[19] Whitehouse D J, Bowen D K, Venkatesh V C, Lonardo P and Brown C A 1994 Gloss and surface topography *CIRP Ann Manuf. Technol.* **43** 541–9

[20] Sandoz P, Tribillon G, Gharbi T and Devillers R 1996 Roughness measurement by confocal microscopy for brightness characterization and surface waviness visibility evaluation *Wear* **201** 186–92

[21] Kuo C-C and Chen Y-R 2011 A new method to characterizing surface roughness of TiO_2 thin films *Opt. Lasers Eng.* **49** 410–4

[22] Kenmochi K, Yarita I, Abe H, Fukuhara A, Komatu T and Kaito H 1997 Effect of micro-defects on the surface brightness of cold-rolled stainless-steel strip *J. Mater. Process. Technol.* **69** 106–11

[23] Antonson S A, Yazici A R, Kilinc E, Antonson D E and Hardigan P C 2011 Comparison of different finishing/polishing systems on surface roughness and gloss of resin composites *J. Dentistry* **39** e9–17

[24] da Costa J, Adams-Belusko A, Riley K and Ferracane J L 2010 The effect of various dentifrices on surface roughness and gloss of resin composites *J. Dentistry* **38** 123–8

[25] Heintze S D, Forjanic M and Rousson V 2006 Surface roughness and gloss of dental materials as a function of force and polishing time *in vitro Dent Mater.* **22** 146–65

[26] Hosoya Y, Shiraishi T, Puppin-Rontani R M and Powers J M 2011 Effects of acidulated phosphate fluoride gel application on surface roughness, gloss and colour of different type resin composites *J. Dentistry* **39** 700–6

[27] Varley R J, Simmonds E K, Seebergh J E and Berry D H 2012 Investigation of factors impacting the in-service degradation of aerospace coatings *Prog. Org. Coat.* **74** 679–86

[28] Singh R K, Chen Z, Kumar D, Cho K and Ollinger M 2002 Critical issues in enhancing brightness in thin film phosphors for flat-panel display applications *Appl. Surf. Sci.* **197–198** 321–4

[29] Järnström J, Ihalainen P, Backfolk K and Peltonen J 2008 Roughness of pigment coatings and its influence on gloss *Appl. Surf. Sci.* **254** 5741–9

[30] ISO 16610-31 2010 *Geometrical Product Specifications (GPS)—Filtration, Part 31: Robust profile filters: Gaussian regression filters* (International Organization for Standardization)

[31] Stout K J, Sullivan P J, Dong W P, Mainsah E, Luo N, Mathia T and Zahouani H 1993 The developments of methods for the characterisation of roughness in three dimensions *Report of the Commission of the European Communities* pp 1–358

[32] ISO 25178-2 2012 *Geometrical Product Specifications (GPS)—Surface texture: Areal, Part 2: Terms, definitions and surface texture parameters*

[33] ISO 13565-1 1996 *Geometrical Product Specifications (GPS)—Surface texture: Profile method, surfaces having stratified functional properties, Part 1: Filtering and general measurement conditions*

[34] Beckmann P and Spizzichino A 1963 *The Scattering of Electromagnetic Waves from Rough Surfaces* (Norwood, MA: Artech House)

[35] Jaggard D L 1997 Fractal electrodynamics: from super antennas to superlattices *Fractals in Engineering* ed J Lévy Véhel, E Lutton and C Tricot (London: Springer) pp 204–21

[36] Sheppard C J R 1996 Scattering by fractal surfaces with an outer scale *Opt. Commun.* **122** 178–88

[37] Jakeman E 1991 Non-Gaussian statistical models for scattering calculations *Waves Random Media* **1** S109–19

[38] Jakeman E 1982 Scattering by a corrugated random surface with fractal slope *J. Phys. A: Math. Gen.* **15** L55

[39] Botet R, Poliakov E Y, Shalaev V M and Markel V A 1997 Fractal-surface-enhanced optical responses *Fractals in Engineering* ed J Lévy Véhel, E Lutton and C Tricot (London: Springer) pp 237–51

[40] Purcell E M and Pennypacker C R 1973 Scattering and absorption of light by nonspherical dielectric grains *Astrophy. J.* **186** 705–14

[41] Draine B T 1988 The discrete-dipole approximation and its application to interstellar graphite grains *Astrophy. J.* **333** 848–72

[42] Brekhovskikh L M 1952 The diffraction of waves by a rough surface. (Part I and II) *Zh Eksp. Teor. Fiz.* **23** 275–305

[43] Nowicki B 1985 Multiparameter representation of surface roughness *Wear* **102** 161–76

[44] Mandelbrot B 1967 How long is the coast of Britain? Statistical self-similarity and fractal dimension *Science* **156** 636–8

[45] Mandelbrot B B 1975 *Les Objets Fractals: Forme, Hasard et Dimension* (Paris, France: Flammarion)

[46] Mandelbrot B B 1983 *The Fractal Geometry of Nature* 3rd edn, vol 173 (New York: Henry Holt and Company)

[47] Gagnepain J J and Roques-Carmes C 1986 Fractal approach to two-dimensional and three-dimensional surface roughness *Wear* **109** 119–26

[48] Majumdar A and Tien C L 1990 Fractal characterization and simulation of rough surfaces *Wear* **136** 313–27

[49] Chesters S, Wang H C and Kasper G A 1991 Fractal-based method for describing surface texture *Solid State Technol.* **34** 73–7
[50] Min S W, Lim S P and Lee K S 1995 A fractal surface and its measurement by computer simulation *Opt. Laser Technol.* **27** 331–3
[51] Bigerelle M, Najjar D and Iost A 2005 Multiscale functional analysis of wear: a fractal model of the grinding process *Wear* **258** 232–9
[52] Bigerelle M, Gautier A, Hagege B, Favergeon J and Bounichane B 2009 Roughness characteristic length scales of belt finished surface *J. Mater. Process. Technol.* **209** 6103–16